Molecular Vision 2016; 22:1387-1404 <http://www.molvis.org/molvis/v22/1387>
Received 15 July 2016 | Accepted 8 December 2016 | Published 10 December 2016

Accumulation of cholesterol and increased demand for zinc in serum-deprived RPE cells

Sanghamitra Mishra,[1] Katherine Peterson,[1] Lili Yin,[1] Alan Berger,[2] Jianguo Fan,[1] Graeme Wistow[1]

(The first two authors contributed equally to this work.)

[1]Section on Molecular Structure and Functional Genomics, National Eye Institute, National Institutes of Health, Bethesda, MD; [2]Lowe Family Genomics Core, Johns Hopkins University - School of Medicine, Baltimore, MD

Purpose: Having observed that confluent ARPE-19 cells (derived from human RPE) survive well in high-glucose serum-free medium (SFM) without further feeding for several days, we investigated the expression profile of RPE cells under the same conditions.

Methods: Expression profiles were examined with microarray and quantitative PCR (qPCR) analyses, followed by western blot analysis of key regulated proteins. The effects of low-density lipoprotein (LDL) and zinc supplementation were examined with qPCR. Immunofluorescence was used to localize the LDL receptor and to examine LDL uptake. Cellular cholesterol levels were measured with filipin binding. Expression patterns in primary fetal RPE cells were compared using qPCR.

Results: Microarray analyses of gene expression in ARPE-19, confirmed with qPCR, showed upregulation of lipid and cholesterol biosynthesis pathways in SFM. At the protein level, the cholesterol synthesis control factor SRBEF2 was activated, and other key lipid synthesis proteins increased. Supplementation of SFM with LDL reversed the upregulation of lipid and cholesterol synthesis genes, but not of cholesterol transport genes. The LDL receptor relocated to the plasma membrane, and LDL uptake was activated by day 5–7 in SFM, suggesting increased demand for cholesterol. Confluent ARPE-19 cells in SFM accumulated intracellular cholesterol, compared with cells supplemented with serum, over 7 days. Over the same time course in SFM, the expression of metallothioneins decreased while the major zinc transporter was upregulated, consistent with a parallel increase in demand for zinc. Supplementation with zinc reversed expression changes for metallothionein genes, but not for other zinc-related genes. Similar patterns of regulation were also seen in primary fetal human RPE cells in SFM.

Conclusions: ARPE-19 cells respond to serum deprivation and starvation with upregulation of the lipid and cholesterol pathways, accumulation of intracellular cholesterol, and increased demand for zinc. Similar trends are seen in primary fetal RPE cells. Cholesterol accumulation basal to RPE is a prominent feature of age-related macular degeneration (AMD), while dietary zinc is protective. It is conceivable that accumulating defects in Bruch's membrane and dysfunction of the choriocapillaris could impede transport between RPE and vasculature in AMD. Thus, this pattern of response to serum deprivation in RPE-derived cells may have relevance for some aspects of the progression of AMD.

The RPE is a polarized monolayer essential to the maintenance of vision [1-3]. The RPE scavenges shed photoreceptor discs, recycles the visual pigment, and mediates traffic between the outer retina and the choriocapillaris, a complex bed of blood vessels underlying the retina and separated from the RPE by Bruch's membrane [4]. The RPE survives with little or no cell turnover while it is subject to various stresses, including light exposure and the accumulation of pigmented materials derived from the RPE's role in recycling components of the visual cycle [1-3].

Age-related macular degeneration (AMD), a major cause of vision loss in aging populations [2,5], is associated with dysfunction of the RPE and with the formation of deposits of proteins (many related to the complement system) and lipids basal to RPE, often in the form of drusen [6,7]. The progression of the disease is generally associated with damage in and around Bruch's membrane and recession of the capillary bed [8,9]. Many systemic and genetic risk factors for AMD have been identified, suggesting that it is a complex disease with multiple initiators and pathways that converge on death for the RPE and photoreceptors [7,10-14]. Several studies have identified cholesterol-rich deposits in AMD [7,15] while population studies have shown that zinc and other dietary factors are protective [16].

In previous work on the interaction of two important AMD-related proteins, EFEMP1/Fibulin 3 (Fib3) and complement factor H (CFH), in deposits in soft drusen in AMD [15], we observed that human RPE-derived ARPE-19 cells [17] survived in high-glucose serum-free medium for 7 days

Correspondence to: Graeme Wistow, Section on Molecular Structure and Functional Genomics, National Eye Institute, Building 6 Room 106, National Institutes of Health, Bethesda, MD 20892; Phone: (301) 402 3452; FAX: (301) 496 0078; email:graeme@helix.nih.gov

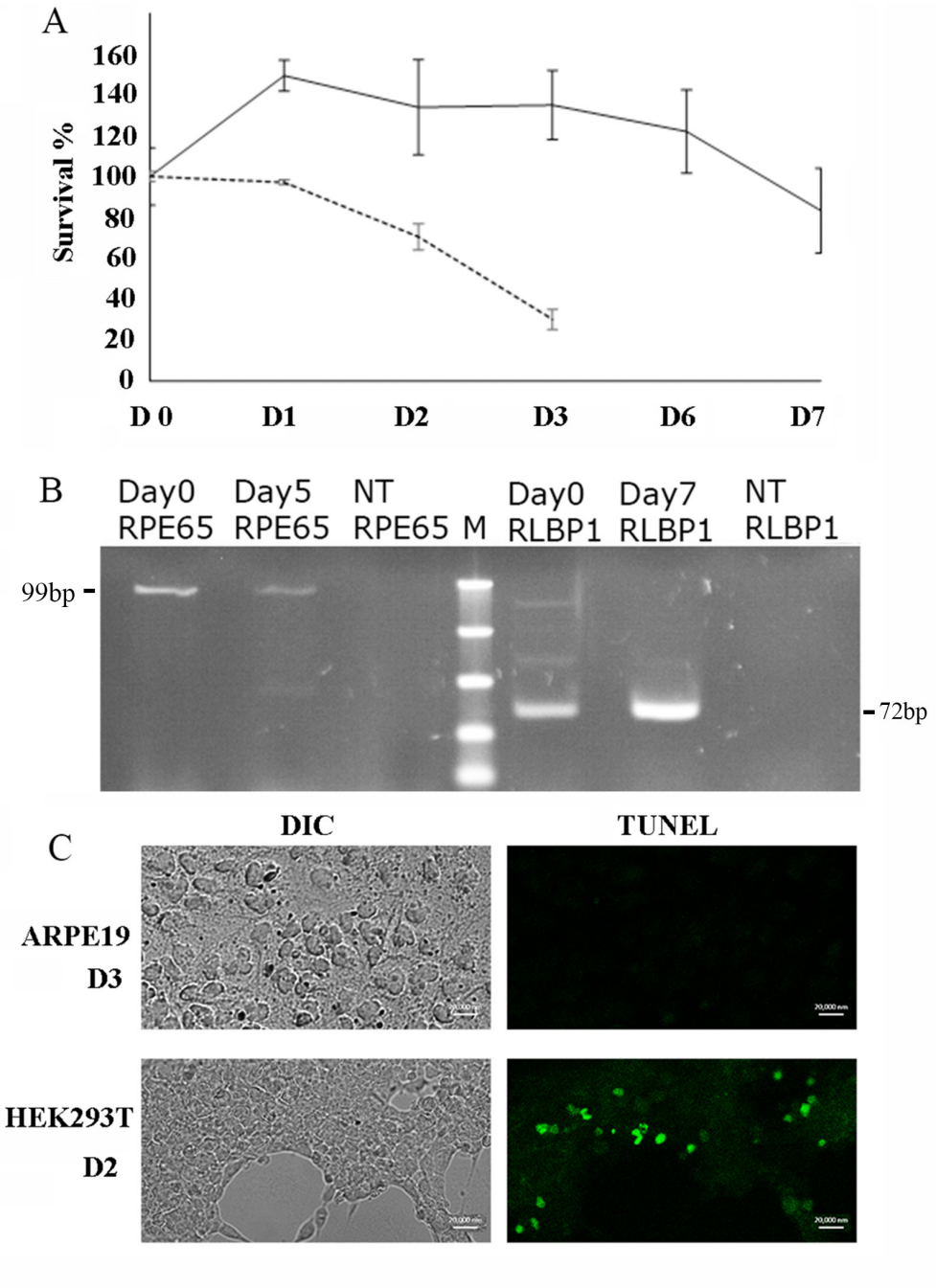

Figure 1. RPE-derived cells survive well in serum-free medium. **A**: The cell survival percentage of ARPE-19 cells (solid line) and human embryonic kidney (HEK293) cells (dashed line) under serum deprivation with standard deviation error bars, compared with day 0 (100%). **B**: Expression of mRNAs of RPE markers, RPE65 and RLBP1, were detected in ARPE-19 cells in serum-free medium (SFM) with PCR. NT is no template control. **C**: HEK293 cells die by apoptosis in SFM, ARPE-19 and HEK293 cells were serum starved, and terminal deoxynucleotidyl transferase dUTP nick end labelin (TUNEL) assay was performed. Confocal Differential interference contrast (DIC; left) and green fluorescence (right) TUNEL images show unstained and apoptotic cells, respectively. Scale bar=20 µM.

without further feeding and that Fib3 secretion was detected after 3 days of treatment. As Fib3 deposition is a common feature of AMD [15,18], we were interested in characterizing the transcriptional profile of confluent ARPE-19 cells under these conditions. ARPE-19 cells are widely used as an investigational model for different aspects of RPE responses [19-24]. Our results show that RPE-derived cells, while maintaining expression of RPE-specific marker genes, respond to serum deprivation or starvation by activating cholesterol and lipid synthesis and transport pathways, accumulate cholesterol, and show increased demand for zinc.

METHODS

Cell culture: Human RPE-derived cells, ARPE-19 [17] (ATCC, Manassas, VA, CRL-2302; passage numbers 19–25), were grown in DMEM/Ham's F12 50/50 Mix with 1.5 mM L-glutamine, 0.8 mM sodium pyruvate, 0.08 mM

non-essential amino acids, penicillin/streptomycin (100 unit penicillin/100 µg streptomycin per ml), and 10% fetal bovine serum (FBS) under 5% CO_2 at 37 °C. Human embryonic kidney cells (HEK293; ATCC CRL-1573™) were grown in DMEM with penicillin/streptomycin (100 unit penicillin/100 µg streptomycin per ml) and 10% FBS under 5% CO_2 at 37 °C. Both cell lines were authenticated using short tandem repeat (STR) analysis by the cell line authentication service (ATCC). Briefly, seventeen short tandem repeat (STR) loci plus the gender determining locus, amelogenin, were amplified using the commercially available PowerPlex 18D Kit from Promega (Madison, WI). The cell line sample was processed using the ABI Prism 3500xl Genetic Analyzer. Data were analyzed using GenMapper ID-X v1.2 software (Applied Biosystems, Madison, WI). Appropriate positive and negative controls were run and confirmed for each sample submitted. The results of STR showed that showed the ARPE-19 sample was a 100% match to the ATCC ARPE-19 cell line, while the HEK293 sample was a 94% match to the ATCC reference HEK293 cell line (CRL-1573). Primary human fetal RPE (hfRPE) [25], ID 12,061,301 (gift of Dr. Miller, NEI, NIH, and prepared under the tenets of the Declaration of Helsinki and the NIH institutional review board), were cultured on Corning Primaria plastic culture ware (Thermo Fisher Scientific, Waltham, MA), as previously described [25]. All cell lines used have been published previously. The cells were free from contamination. ARPE-19 and hfRPE cells were validated for the expression of the RPE65 and RLBP1 marker genes [17] with PCR of cDNA using the RPE65-specific primers 5′-CCA GAT GCC TTG GAA GAA GA-3′; 5′-CTT GGC ATT CAG AAT CAG GAG-3′ (99 bp amplicon) and the RLBP-specific primers 5′-AGA TCT CAG GAA GAT GGT GGA C-3′; 5′-TGG ATG AAG TGG ATG GCT TT-3′ (72 bp amplicon).

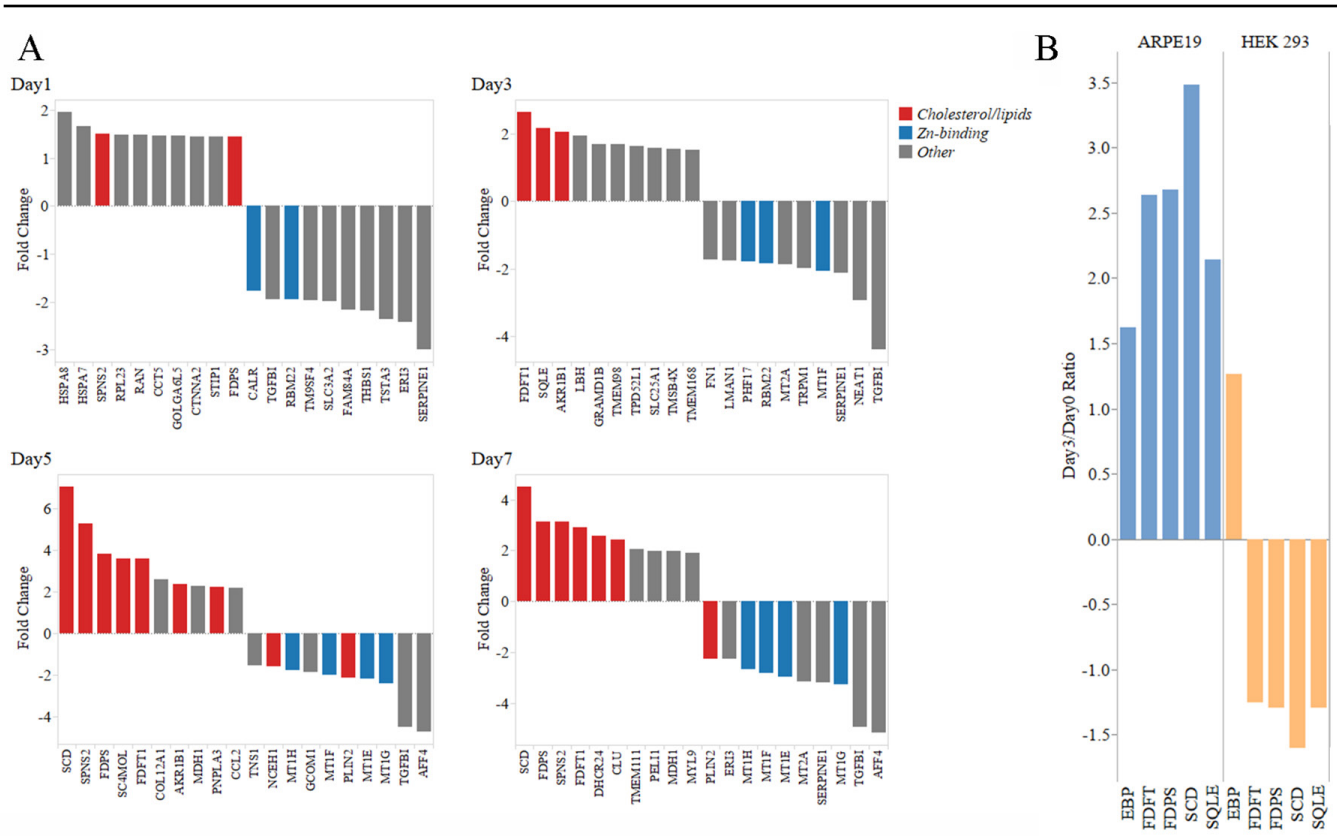

Figure 2. Genes for lipid synthetic pathways and zinc-binding proteins are prominent among DEGs in ARPE-19 in serum-free medium. **A**: Gene expression results measured by microarrays for serum deprived ARPE-19 cells compared to Day0 serum supplemented cultures. Bars represent the ratio of gene expression. Results are filtered for p values less than 0.05 and fold-change values greater than 1.2. The top 10 up and downregulated genes are shown. The bars are colored to identify genes classified as cholesterol/lipid or Zn-binding. Interactive figures, using Tableau Software (Seattle, WA), for the complete DEG (Interactive Figures). **B**: Comparison of the effect of serum deprivation on gene expression in ARPE-19 versus human embryonic kidney (HEK293T) cells. Key genes in the cholesterol/lipid pathway have increased expression at 3 days in serum-free medium (SFM) in ARPE-19 cells but not in HEK293T cells. Gene expression is measured as the ratio of day 0 serum-supplemented cultures and serum-starved cultures with microarray hybridization.

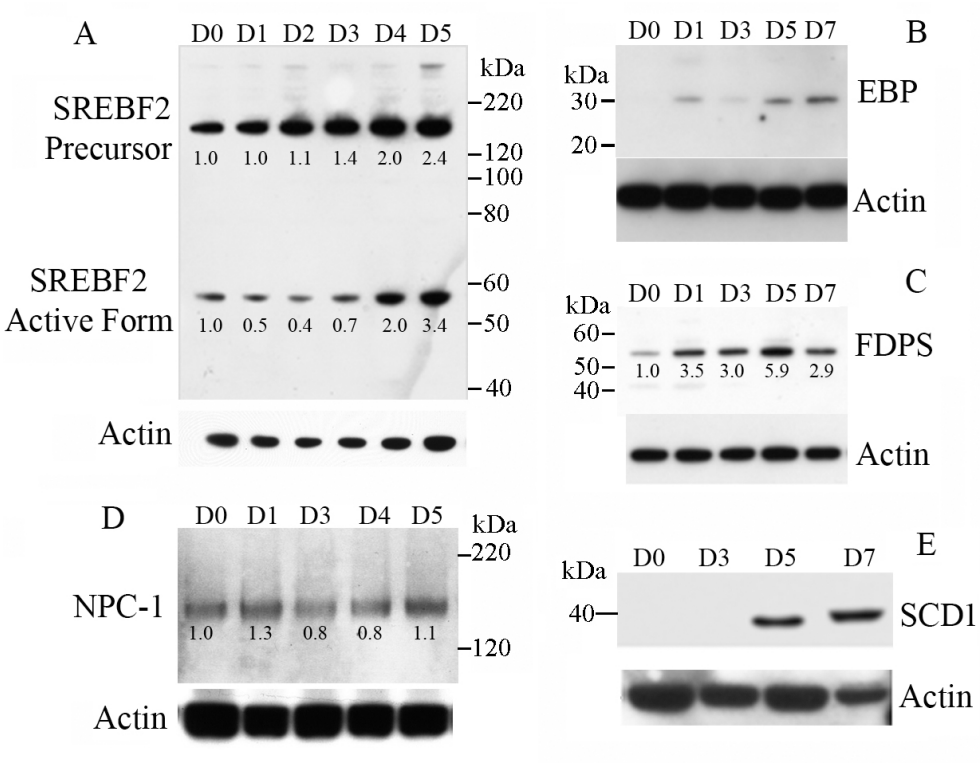

Figure 3. Lipid synthetic and transport proteins are induced in ARPE-19 cells in SFM. Western blots of ARPE-19 cell lysates after the indicated number for days in serum-free medium (SFM) are shown for (**A**) SREBF2, (**B**) EBP, (**C**) FDPS, (**D**) NPC1 and (**E**) SCD1 (upper panels). The same blots were stripped and probed with anti-β-actin to indicate loading controls (lower panels). Blots are representative of two to three replications each. For the bands that showed progressive increases, the blots were scanned and quantitated using ImageJ and normalized to actin loading controls, setting day 0 to the value 1.

For serum deprivation, growth medium was removed; the cells were washed once and kept in serum-free medium (SFM), Dulbecco's Modified Eagle Medium (Gibco Life Technology, Gaithersburg MD: catalog#12634; DMEM) with 1% penicillin/streptomycin (100 unit penicillin/100 µg streptomycin per ml). All time points ended on the same day, by treating the wells with the longest duration earliest and so on. Day 0 in all experiments refers to the cells that remained in serum-containing medium throughout the experiment.

For supplementation with low-density lipoprotein (LDL), the cells were washed once with SFM and incubated in 50 µg/ml LDL diluted in SFM and filtered through a 0.22 µg filter. For supplementation with zinc, $ZnCl_2$ was prepared in a 50 µM concentration in SFM and filtered through a 0.22 µg filter and added to cells.

Cell viability assay: Cells were plated in 96-well plates. Following the serum deprivation treatment, the medium was removed from all wells, and 110 µl of 10% CCK-8 reagent (Dojindo Molecular Technologies Inc., Rockville, MD) in SFM was added to all wells, including the cell-free blank wells. The plates were incubated at 37 °C for 1 h. Then optical density (OD) 450 nm was measured. The survival percentage for each day was calculated relative to the absorbance of day 0, taken as 100%. Each survival percentage is the average reading of eight wells from three separate plates.

Protein isolation: Treated cells were washed once with 1X phosphate-buffered saline (PBS; KD Medical, Columbia MD: catalog# RGF-3190) detached from the culture dish in 1 ml of 1X PBS using a cell lifter, and pelleted at 400 × *g* for 10 min at 4 °C. Cell pellets were lysed on ice in radioimmunoprecipitation assay (RIPA) buffer (25 mM Tris-HCl, pH 7.6), 150 mM NaCl, 1% NP-40, 1% sodium deoxycholate, and 0.1% sodium dodecyl sulfate (SDS) with a Halt protease inhibitor cocktail (Thermo Fisher Scientific), for 1 h, vortexing every 15 min. The lysate was then centrifuged at 12,000 ×*g*, and the supernatant was used for the western blot analysis. The protein concentration was estimated using the Bicinchoninic Acid Protein Assay (BCA) kit (Thermo Fisher Scientific).

Immunoblotting: Equal concentrations of total protein in cell lysates were resolved on SDS–PAGE (PAGE) and transferred to a polyvinylidene difluoride (PVDF) membrane. All incubations and washing for western blotting were done on a rocking platform. Blots were blocked with 5% nonfat milk in Tris-buffered saline with Tween-20 (TBST; 20 mM Tris, pH 7.4, 150 mM NaCl with 0.1% Tween-20) rinsed once in TBST and incubated with primary antibody diluted in TBST at 4 °C overnight. The blots were washed twice, 10 min at room temperature in TBST, and incubated in horseradish peroxide (HRP)-conjugated secondary antibodies diluted in TBST for 1 h at room temperature. The blots were then washed twice,

10 min each wash at room temperature with TBST, and the protein bands were detected using the LumiGold ECL Western Blotting Detection Kit (VerII; Signagen Laboratories, Ijamsville, MD). The blots shown are representative of at least three biologic repeats of each experiment. Relative quantitation of the proteins was performed using ImageJ software (National Institutes of Health, Bethesda, MD). The relative quantity of the signal from β-actin was determined per lane as a ratio compared to day 0. The β-actin level was then used to normalize the signal from the other proteins, also calculated as the ratio compared to day 0.

The following commercially provided and validated antibodies were used at the recommended dilutions for immunoblotting or immunolabeling: rabbit polyclonal anti-SREBF2 ab30682 (Abcam, Cambridge, UK); rabbit polyclonal anti-SCD1 ab23331 (Abcam), rabbit polyclonal anti-emopamil binding protein (EMP) ab105374 (Abcam), rabbit polyclonal anti-FDPS ab38854 (Abcam); rabbit polyclonal anti-Neimann Pick C1 (NPC1) ab108921 (Abcam), mouse monoclonal anti-β-actin AC-15 A1978 (Sigma Aldrich, St. Louis, MO), rabbit polyclonal anti-SLC39A1 NBP1–76498 (Novus Biologicals, Littleton, CO), and rabbit polyclonal anti-LDL receptor (LDLR) 10,012,422 (Cayman Chemical, Ann Arbor, MI). Secondary antibodies included goat anti-rabbit HRP ab 6721 (Abcam) and goat anti-mouse HRP ab97040 (Abcam).

Human cDNA microarrays: Gene expression ratios for three biologic replicates of the time series of serum deprivation of ARPE-19 cells were measured using custom cDNA microarrays. Plates of confluent ARPE-19 cells were transferred to SFM and cultured for 7 days. RNA was isolated from the cultures on days 0, 1, 3, 5, and 7 using Trizol® (Thermo Fisher Scientific) following the manufacturer's protocol followed by a clean-up step using the Qiagen RNeasy Mini Kit (Qiagen Inc., Valencia, CA). The quality of the isolated RNAs was measured using an Agilent BioAnalyzer 2100 to determine the RNA integrity number (RIN) of each sample (Agilent Inc., Santa Clara, CA).

The RNAs isolated from the day 0 cultures were pooled for each biologic replicate to provide a single consistent comparison measure. Using the day 0 sample for comparison, we determined the RNA expression ratios for days 1, 3, 5, and 7 with competitive hybridization. Each array was probed with cDNA generated from two RNA samples: a day 0 sample and one of the other days labeled with aminoallyl 2'-deoxyuridine

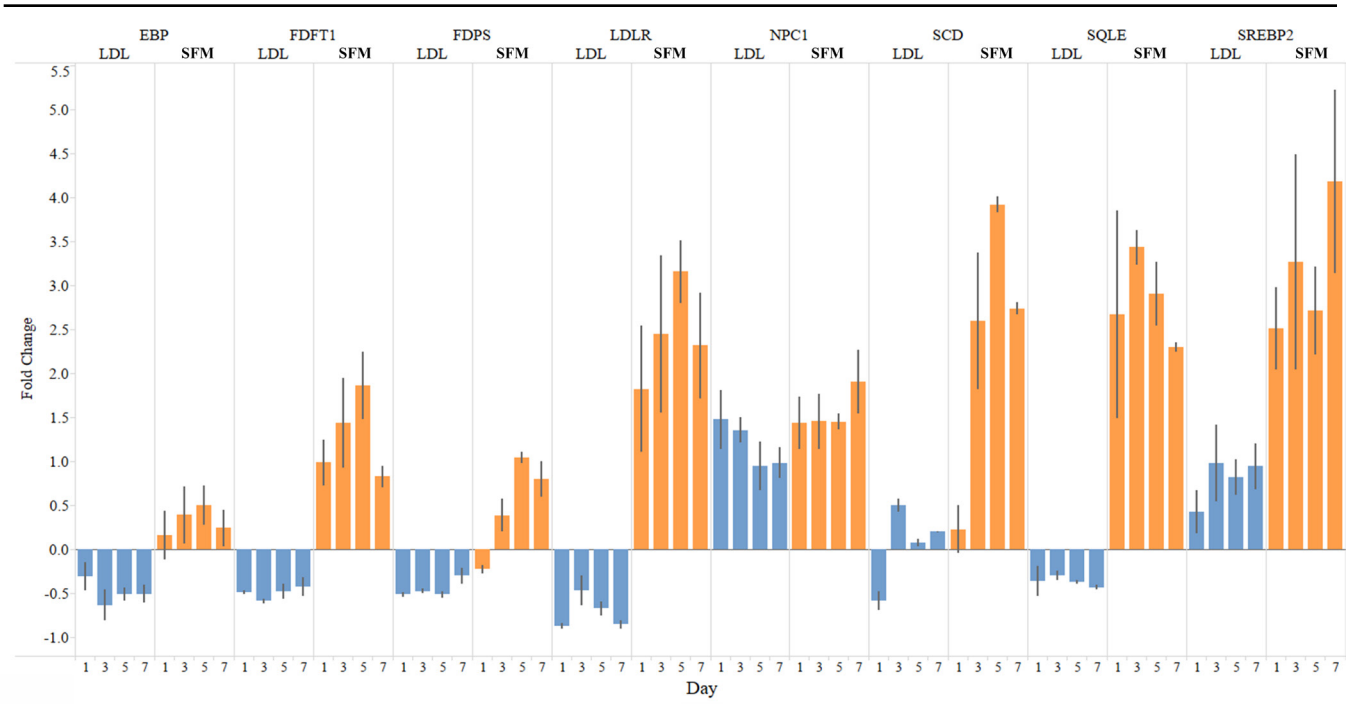

Figure 4. Increased expression of genes in cholesterol and lipid pathways SFM is blocked by supplementation with LDL. Quantitative PCR (qPCR) measures of gene expression from serum-free medium (SFM) ARPE-19 cultures without and with added low-density lipoprotein (LDL; 50 µg/ml) compared to day 0 serum-supplemented cultures. Relative quantity (RQ) values were calculated using the $-\Delta\Delta C_t$ method and normalized using the mean value of four reference transcripts. Fold change=($2^{\wedge} - \Delta\Delta C_t$). Error bars represent the standard error of the mean (SEM; n=3).

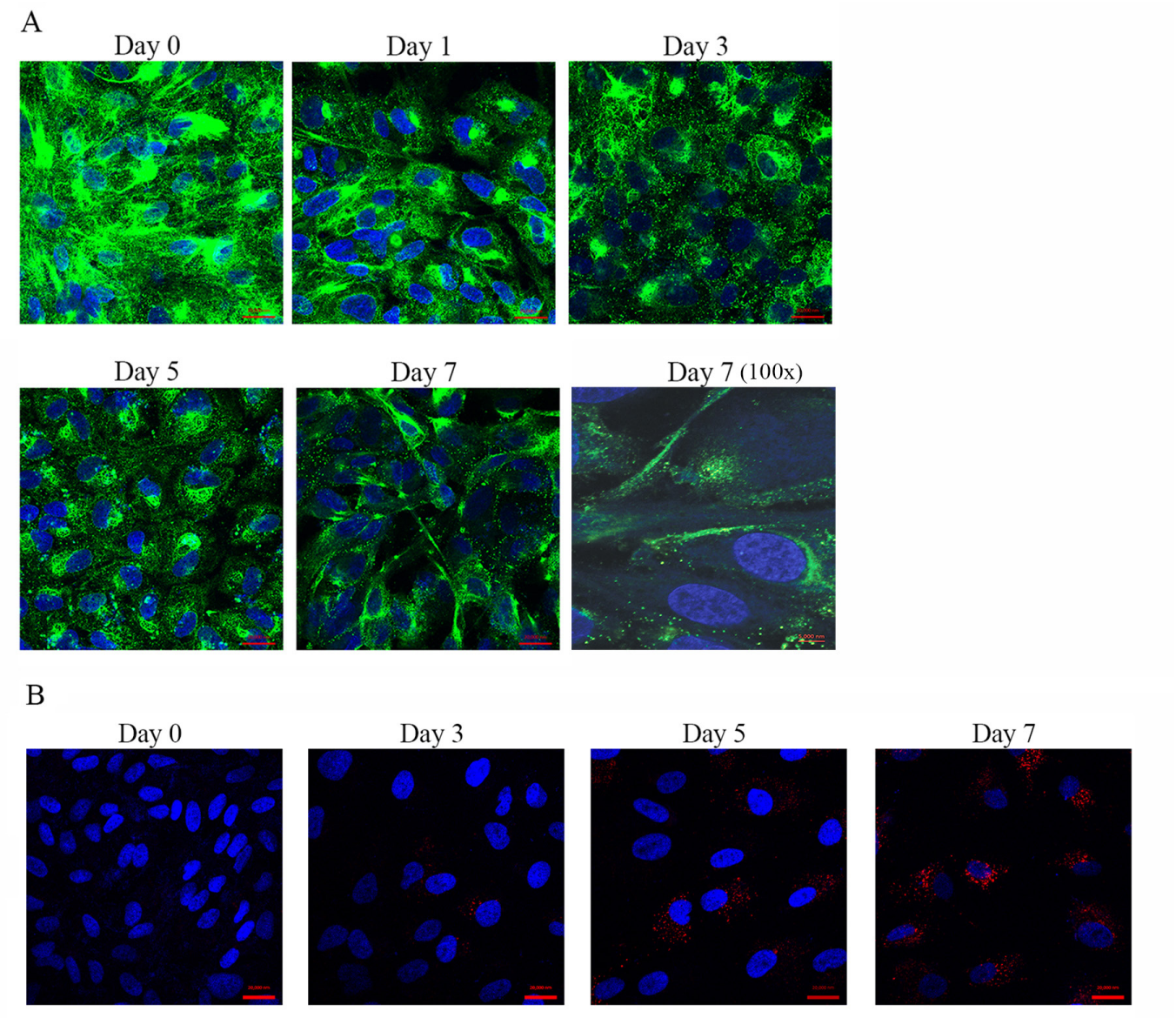

Figure 5. LDLR localization and LDL uptake in serum-deprived and -starved ARPE-19 cells. **A**: Immunofluorescence of cells in serum-free medium (SFM) from day 0–7. Low-density lipoprotein receptor (LDLR; green) is primarily intracellular at day 0, but by day 7 in SFM, more signal appears localized to the cell surface. Images are 40X with scale bar indicating 20 µM, except the final panel with 100X magnification for day 7. Scale bar=5 µM. Nuclei are stained with 4',6-diamidino-2-phenylindole (DAPI; blue). **B**: Uptake of labeled LDL by ARPE-19 cells in SFM. ARPE-19 cells in SFM were incubated with LDL-DyLight 549, washed and fixed, and the nuclei were stained with DAPI (blue). Confocal images show intracellular LDL-DyLight 549 in red. Scale bars=20 µm.

5′-triphosphate (dUTP) cross-linked to either Alexa Fluor 555 (green) or Alexa Fluor 647 (red) fluorescent dye (Molecular Probes, Eugene, OR). The cDNAs were generated using a $d(N)_{15}$ primer (Eurofins MWG, Operon, Huntsville, AL) and SuperScript II reverse transcriptase (Invitrogen, Inc.).

The red and green fluorescent dyes were evenly distributed among the technical replicate samples to mitigate dye bias. For each biologic replicate, the cDNA from each day's sample was hybridized to four arrays, two each labeled with Alexa Fluor 555 and Alexa Fluor 647. For the complete experiment, each day sample (1, 3, 5, and 7) was hybridized to 12 arrays. For comparison, the expression ratios of the day 3

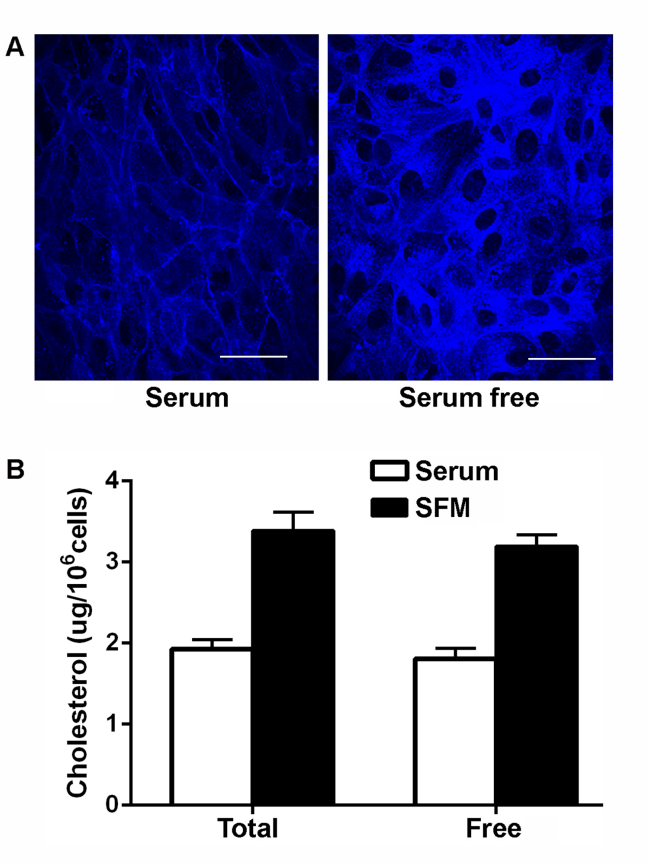

Figure 6. Serum deprivation treatment increases intracellular cholesterol in ARPE-19 cells. **A**: Confocal images of Transwells with confluent ARPE-19 cells stained for cholesterol with filipin (blue). The left panel shows cells in serum containing medium (serum); the right panel shows cells in serum-free medium (serum free) for 7 days before staining. Maximum intensity projections from confocal z-series at 40X magnification are shown. Identical settings were used for both images. Scale bars=50 µm. **B**: Quantitation of free and total cholesterol. Serum-free treatment increases total cholesterol and free cholesterol levels in confluent ARPE-19 cells relative to cells grown in serum (n=4, mean ± standard error of the mean [SEM]).

to day 0 samples from the serum-starved HEK293 cells were determined using microarrays as described above.

Hybridization of the labeled samples to the arrays was performed overnight in a MAUI mixing incubator (Biomicro, Salt lake City, UT). Next, the arrays were washed, dried, and scanned in a ScanArray Express (Perkin Elmer, Waltham, MA) measuring green (A565) and red (A670) fluorescence. The scanned images were analyzed using BlueFuse image analysis software (Illumina, San Diego, CA) to determine the expression ratios of the array features. The images were adjusted for equivalent brightness in each channel and normalized using the Global Lowess option. The image analysis produced gene expression ratios for each array feature.

Differentially expressed genes were identified with a *t* test of the ratios for each day sample. Setting the p value and fold change cut-offs to 0.05- and 1.2-fold, respectively, produced a differentially expressed gene (DEG) list of 722 probes corresponding to 621 genes. Applying a multiple test correction to these data proved too stringent. Therefore, we continued the analyses without applying a correction, reasoning that the hypotheses generated from the analysis of the DEGs would be tested or confirmed with additional independent tests (Appendix 1, Appendix 2, and Appendix 3).

Informatics analysis of gene expression: The gene expression results were subjected to multiple analyses to identify the pathways affected by serum deprivation: Ingenuity Pathways Analysis (IPA) software, to map ontologies represented in the DEG list; DAVID, to identify statistically over- or under-represented pathways in the DEG list from public domain sources, such as Gene Ontology (GO) and Kyoto Encyclopedia of Genes and Genomes (KEGG); and sorting and identifying functionally related genes by examining their *Entrez* descriptions and GO annotations.

qPCR: Hydrolysis probe quantitative PCR (qPCR), TaqMan assays, were used to confirm the array results and quantitate the RNA expression levels in follow-on experiments or for genes that were not present on the array. RNA isolated from the cell cultures was reverse transcribed (Transcriptor First Strand cDNA Synthesis Kit, Roche Applied Sciences, Madison, WI). Assays for each gene were designed using the Universal ProbeLibrary Assay Design website. Custom synthesized primers were purchased from Eurofins MWG Operon. Fluorescent probes were either included in the Universal ProbeLibrary Set or purchased individually from Roche Applied Science.

Using the ABI PRISM® HT7900 real-time PCR system and FastStart Universal Probe Master (ROX; Roche Applied Sciences), the qPCR assays were performed on equivalent samples of cDNA from the time series and normalized to genes whose expression values remained relatively constant throughout. The genes for normalization were selected empirically by comparing their expression values during the time course. Reaction mixes contained 50–250 ng cDNA, 900 nM of each forward/reverse primer, 250 nM Hydrolysis probe, and 1X master mix in a total of 10.6 µl. After a pre-incubation for 10 min at 95 °C there were 40 cycles of 95 °C for 15 s, 60 °C for 1 min, with a single measure at the end of each cycle. Each of the various qPCR experiments employed the combined values from three to four gene assays for normalization. See Appendix 4 for the probe and primer information. Data analysis was performed using ABI SDS (v2.4) and DataAssist (v3.1) software (Applied Biosystems)

following the manufacturer's instructions using the $2^{-\Delta\Delta Ct}$ method [26]. For the ARPE-19 cells, three biologic and three technical replicates were performed for all genes. For the fetal cells, four technical replicates were performed.

LDL uptake assay: LDL uptake was measured using the LDL uptake cell-based assay kit (Cayman Chemical, Applied Biosystems). ARPE-19 cells were grown on Nunc Lab-Tek coverslips (Thermo Scientific) for a 7 day course of serum deprivation or for a course of serum starvation supplemented with 50 µg/ml unlabeled human LDL (Intracel, Frederick, MD). A set of cells were serum deprived in replicate to monitor the LDLR with immunofluorescence. Media replacement and continuing serum deprivation were organized so that all of the samples were ready for assay on a single day. On the day of the assay, the cells were washed once with SFM followed by incubation in a 1:100 solution of LDL DyLight 549 (Thermo Fisher Scientific) working solution in SFM for 3 h. Post-treatment, the cells were washed with PBS (137 mM NaCl, 10 mM phosphate, 2.7 mM KCl; pH of 7.4) and fixed in 4% paraformaldehyde in PBS for 10 min, mounted, and visualized using a LSM 700 confocal microscope (Carl Zeiss Vison Inc., San Diego, CA).

LDL receptor localization: ARPE-19 cells were grown on chambered slides in SFM for 7 days. On the day of assay, the medium was removed, and the cells were washed with PBS and fixed with Cell-Based Assay Fixative Solution. Following fixation, the cells were washed three times for 5 min each in TBST and then incubated for 30 min in blocking solution. Next, the cells were incubated with rabbit anti-LDL receptor diluted 1:100 in TBST for 1 h at room temperature. The cells were washed three times in TBST for 5 min each and incubated with DyLight 488-conjugated goat anti-rabbit immunoglobulin G (IgG), 1:100 in TBST at room temperature in the dark for 1 h. Finally, the cells were washed three times for 5 min each in TBST and mounted. Results of the assay were visualized using a Zeiss LSM 700 confocal microscope. Mounted slides were saved for up to 3 days in a moist chamber at 4 °C.

Filipin labeling: ARPE-19 cells were grown on a Nunc® Lab-Tek® Chamber (Sigma-Aldrich) in DMEM with 10%

Table 1. Selected zinc binding protein genes significantly regulated during the course of serum deprivation.

Gene	Function	Day (p value)
FBLIM1	Cell-extracellular matrix interactions, contributes to prevention of apoptosis of epithelial cells through extracellular matrix adhesion [54]	D 7 +1.2-fold (0.0023)
FASN	Cholesterol, triglyceride, and fatty acid homeostasis, insulin signaling and estrogen response, VitaminB5 metabolism, and fatty acyl-CoA biosynthesis, downregulation is associated with hypoxic cell death in HepG2 [55]	D5 +1.26-fold (0.0023) D7 +1.22-fold (0.0072)
RFWD2	Modulator of FASN activity, E3-ligase for p53 [56] and may play a role in responses to UV damage in mammalian cells, including regulating autophagy [57,58]	D5 +1.39-fold (0.0143)
RPS6KA5	An NF-κB RelA/p65 kinase, part of the innate immune system, mediates activation of pro-inflammatory genes, and regulates cigarette smoke-induced histone modifications on NF-κB-dependent genes [59]. Cigarette smoking is a risk factor for AMD [60,61]	D5 +1.46-fold (0.0307) D7 +1.51-fold (0.0112)
NR2C2	Plays a role in protecting cells from oxidative stress and damage induced by ionizing radiation. Associated with AMD-risk through linkage analyses [62] which implicated stress-activated MAPK pathway constituents with AMD risk.	D7 +1.37-fold (0.0106)
GLIS2	Associated with kidney defects, including basement membrane thickening and increased apoptosis and upregulation of complement proteins CFH and C3, in mice. Glis2mut mice showed increased expression of genes involved in immune responses/inflammation and fibrosis/tissue remodeling in kidneys [63,64].	D5 −1.3-fold (0.0439)
JADE1	Pro-apoptotic ubiquitin ligase [65]	D3 −1.8-fold (0.0497) D7 −1.38-fold (0.0269)
VPS11	Vesicle trafficking and formation of late endosomes, required for maintenance of RPE in a vertebrate model [66]	D1 +1.26-fold (0.0035)
ZNF418	Suppressor of the MAPK pathway [67]	D7 +1.38-fold (0.0444)
ZXDC	Transcription factor that activates CCL2, a chemokine that has been implicated in age-related retinal degeneration [68]	D7 −2.24-fold (0.0126)

Official gene symbols followed by a brief functional description of the zinc binding protein. The last column provides the day with the relative increase or decrease as compared to day0 and the associated p value from *t* test results for time points with significant differential expression.

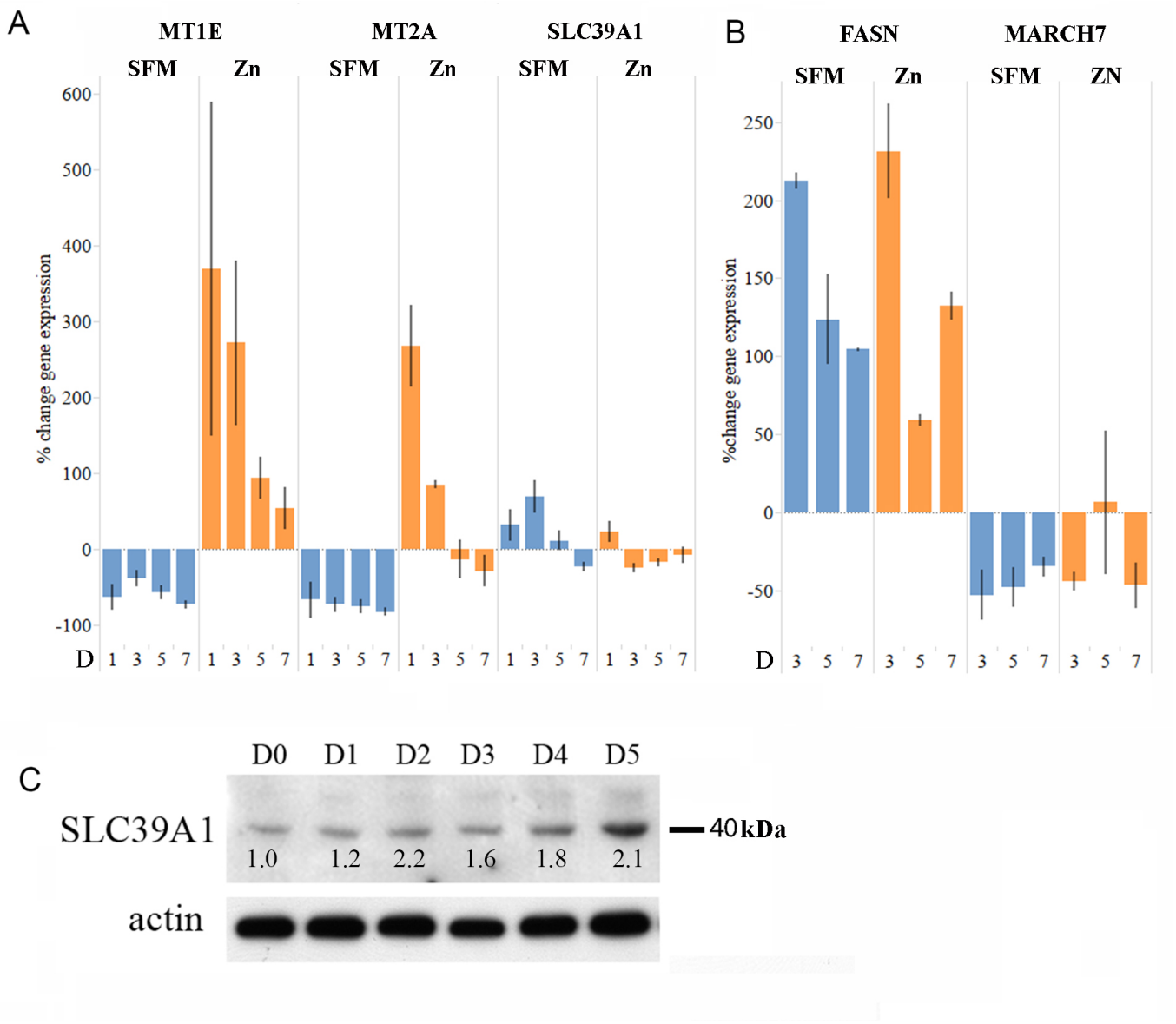

Figure 7. The effect of serum deprivation and zinc supplementation on the expression of genes that encode ZBPs. Gene expression values were measured with quantitative PCR (qPCR) and Relative quantity (RQ) values were calculated using the $-\Delta\Delta C_t$ method and normalized using the mean value of three reference transcripts. Percent change=(RQ–1) × 100. Error bars represent the standard error of the mean (n=3). **A**: Metallothionein expression decreases in serum-free medium (SFM), and this is reversed by supplementation with zinc. **B**: SFM-regulated expression of other zinc-binding protein (ZBP) genes is not affected by the addition of supplemental zinc. **C**: Expression of the zinc transporter ZIP1/SLC39A1 in SFM. Western blot of ARPE-19 cell lysates, prepared after serum deprivation for the indicated number of days, with rabbit polyclonal anti-SLC39A1 antibody. The same blot stripped and reprobed with anti-actin-horseradish-peroxidase (HRP) antibody is shown below as the loading control. Normalized levels relative to day 0, as described in legend to Figure 3, are shown numerically.

serum. When the cells were nearly confluent, the medium was replaced with either serum-containing or serum-free medium for 6 days. Serum-containing or SFM was added to the chambers. After treatment, the medium was removed; the cells were washed once with TBS and fixed with 4% paraformaldehyde (PFA) for 10–15 min at room temperature. Fixed cells were washed once with TBS with 0.1% Polysorbate 20 and twice with TBS for 5 min each. One milligram filipin was dissolved in 200 µl ethanol, aliquoted at 20 µl, and desiccated under argon. Each aliquot was diluted to 0.05 mg/ml in TBS. Diluted filipin was added to each well and incubated in the dark for 60 min. Following filipin labeling, the cells were washed once with TBS and incubated with 1:300 Topro-3 (Molecular Probes) in TBS for 30 min in the dark at

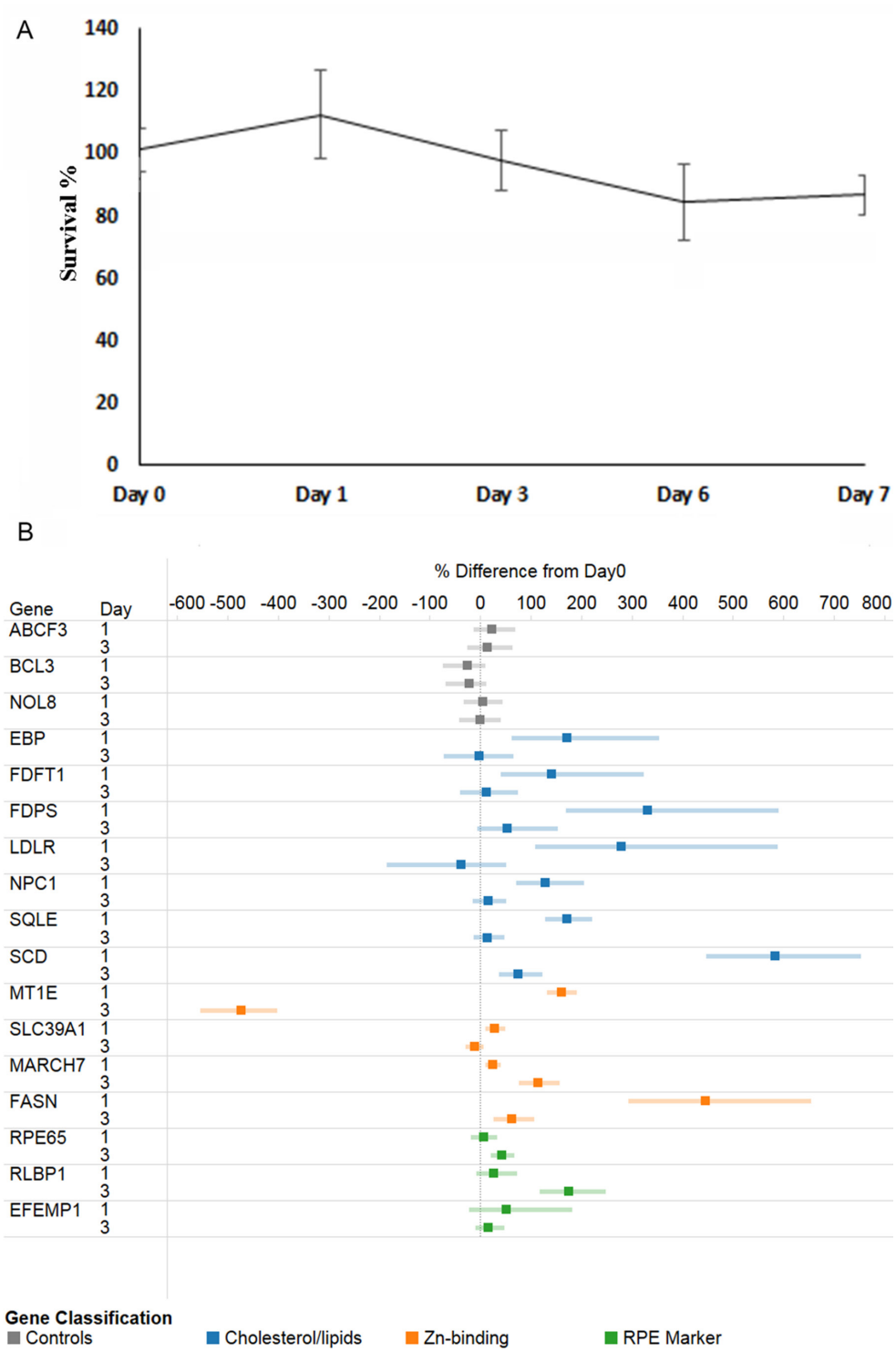

Figure 8. Primary hfRPE cells in SFM. **A**: Cell survival percentage of human fetal RPE (hfRPE) cells in serum-free medium (SFM) over several days with standard deviation error bars compared with day 0 (100%). **B**: Gene expression ratios of serum-starved hfRPE cultures compared to day 0 serum-supplemented hfRPE cultures measured with quantitative PCR (qPCR) for selected genes. Points to the left of 0 indicate decreased expression as a percentage compared to day 0; points to the right indicate increased expression. Relative quantity (RQ) values for triplicate assays were calculated using the $-\Delta\Delta C_t$ method and normalized using the mean value of three reference transcripts. Percent change=(RQ–1) × 100.

room temperature. After that, the cells were washed in the dark three times with TBS and mounted with Prolong Gold (Molecular Probes). Staining was immediately visualized using a FV1000 confocal microscope (Olympus America Inc., Center Valley, PA).

Cholesterol quantitation: Cholesterol levels were determined using the Cholesterol/Cholesteryl Ester Quantification Kit from Abcam Inc. (Toronto, Canada). Briefly, 5 × 10^6 cells were harvested and washed with cold PBS. Cells were extracted in 1,000 µl chloroform:isopropanol:NP-40

Table 2. Differentially expressed genes from serum starvation of ARPE-19 cells with known associations to eye disease with OMIM identifications.

Gene	*Entrez*ID	OMIM	Disease
ABCA4	24	248,200	Stargardt disease 1
		153,800	age-related macular degeneration 2
		604,116	cone-rod dystrophy 3
		601,718	retinitis pigmentosa 19
CHM	1121	303,100	choroideremia
COL5A2	1290	130,000	Ehlers-Danlos syndrome, type I
CRYBB1	1414	600,929	cataract, pulvreulent included
HPS1	3257	203,300	Hermansky-Pudlak syndrome 1
NR2C2	7182		risk for AMD
PDE6A	5145	180,071	retinitis pigmentosa, autosomal recessive
PITPNA	5306		retinal degeneration
PPT1	5538	256,730	neuronal ceroid lipofuscinosis 1
PROM1	8842	603,786	Stargardt disease 4
		604,365	autosomal recessive retinal degeneration
		608,051	retinal bull's eye macular dystrophy 2
		604,365	retinitis pigmentosa 41
SOD2	6648		macular degeneration

(7:11:0.1) using a Polytron PT 1200 E homogenizer (Kinematica, Bohemia, NY) followed by centrifugation for 10 min at 15,000 × *g*. The organic phase was carefully transferred to a new tube and dried in vacuum centrifuge at 50 °C. Lipids were dissolved in 200 µl of assay buffer with vortexing. Ten microliter samples were added to a 96-well clear microplate and assayed at 570 nm using a Bio-Rad 680 reader (Bio Rad laboratories, Hercules, CA). Assays were performed in quadruplicate (n=4).

RESULTS

Serum deprivation of ARPE-19 cells: ARPE-19 cells in culture maintain many features of the native RPE in terms of the morphology and expression of tissue-specific marker genes [17] and have been widely used to explore the responses of the RPE-derived cells [27-29]. We previously established conditions that supported confluent ARPE-19 cells under serum deprivation [15]. These conditions were repeated for ARPE-19 and for HEK293 cells. As before, the ARPE-19 cells survived in high-glucose SFM for 7 days (Figure 1A). RT–PCR showed expression of the RPE marker genes RPE65 and RLBP1 at day 0, continuing after several days in SFM (Figure 1B). In contrast, HEK293 in the same high-glucose SFM began to die by day 2 (Figure 1A). Terminal deoxynucleotidyl transferase dUTP nick end labeling (TUNEL) staining showed that HEK293 cells were dying through apoptosis by day 2 while the ARPE-19 cells showed no evidence of apoptosis even at day 3 (Figure 1C).

Gene expression: To look for possible patterns of transcriptional regulation, expression profiles for ARPE-19 and HEK293 cells in SFM were examined using an available custom cDNA microarray derived from the multiple human eye tissue libraries of NEIBank [30,31], representing more than 9,000 eye-expressed human gene transcripts (Appendix 1 and Appendix 2). Probes derived from high-quality mRNA (RIN >9) were prepared for cells at several time points and used for array hybridization. The expression values for each gene were compared with day 0 in SFM. For p values of less than 0.05 and fold changes >1.2 or < −1.2 a differentially expressed gene (DEG) list of 621 unique genes for the serum-deprived ARPE-19 cells was produced (Appendix 3). Analysis of these initial results showed that cholesterol and lipid synthesis pathways were the most prominently upregulated class among the DEGs (Figure 2, Appendix 3). In contrast, key lipid synthesis genes that were upregulated in ARPE-19 cells by day 3 were downregulated in HEK293 (Figure 2B), suggesting that this induction is not a general cellular response to serum deprivation. Another large class of DEGs consisted of genes for zinc-binding proteins (ZBPs; Appendix 3). The RPE-specific marker genes, RPE65 and RLBP1, were detected with the arrays throughout the experiment but varied in level and did not pass the *t* tests for differential expression.

To confirm the array results for ARPE-19 in SFM, 24 DEGs were selected for assay with qPCR. The selection included genes for cholesterol and lipid pathways and zinc-binding and transport proteins, as well as representative antioxidant, inflammation, stress response, tubulin, and extracellular matrix protein genes (Appendix 5). Seventeen of the 24 genes assayed confirmed the array results, most notably the cholesterol and lipid pathway genes and the zinc-binding and transport genes. Five of the qPCR assays, including those for the *α1-tubulin*, *extracellular matrix (ECM)*, and *clusterin-like 1 genes*, failed to confirm the array results or produced ambiguous results. Although previous studies showed increased secretion of EFEMP1/Fib3 protein into the medium during serum deprivation [15], the transcript levels for this gene were not differentially regulated. This suggests that any regulation of Fib3 secretion in SFM occurs post-transcriptionally.

To further confirm the induction of cholesterol and lipid pathway genes in SFM, the levels of several key proteins were examined with western blotting (Figure 3). Cholesterol synthesis is regulated by the factor SREBF2 (also known as SREBP2) [32,33]. SREBF2, which is anchored in the endoplasmic reticulum, is activated by proteolysis and translocated to the nucleus where SREBF2 activates a suite of target genes. Western blotting of SREBF2 confirmed that the precursor and activated form increased in abundance in the ARPE-19 cells in SFM by day 4 (Figure 3). Among the key enzymes of cholesterol and lipid synthesis, the farnesyl diphosphate synthase (FDPS) levels increased steadily from day 1 to day 5, emopamil binding protein (EBP) was undetectable at day 0 but increased by day 5, and stearoyl-CoA desaturase-1 (SCD1) was also undetected at day 0 but appeared strongly expressed by day 5. Neimann Pick C1 (NPC1), a cholesterol transporter, was steadily expressed from day 0 to day 7.

LDL supplementation and uptake: To test the effect of cholesterol and lipids on gene expression in ARPE-19 cells in SFM, experiments were repeated with a parallel set supplemented with 50 µg/ml LDL (Figure 4). Initially, a range of concentrations of LDL were tested, based on the manufacturer's recommendations (Intracel), and this concentration was chosen to reflect a physiologically relevant level with minimal toxic effects on the cells. The SFM-associated induction of the cholesterol and lipid synthesis pathway genes was abolished with LDL supplementation, suggesting that the induction was a response to cholesterol and lipid requirements and was not related to experimental procedures, such as the transfer to SFM. In contrast, the level of the cholesterol transporter NPC1 remained elevated, suggesting that intracellular trafficking of cholesterol continued [34], consistent with an increased requirement for cholesterol in the ARPE-19 cells in SFM.

These data suggested that the response of ARPE-19 cells to serum deprivation includes increased demand for cholesterol-related lipids. Next, we examined the distribution of a major factor for cholesterol uptake, the LDL receptor (LDLR), during serum deprivation of ARPE-19 cells using immunofluorescence (IF) labeling. At day 1, most of the IF signal for the LDLR was localized internally, mainly in the Golgi apparatus (Figure 5A). Over time, the LDLR intracellular levels decreased, consistent with activation of the receptor, while by day 7 many cells showed increased labeling of the plasma membrane. To test the uptake of LDL by the cells in SFM, they were serum deprived for 1, 3, 5, and 7 days and incubated with DyLight 549 conjugated LDL. After 1 h, the cells were washed and examined with fluorescence microscopy (Figure 5B). For the first 3 days, there was little evidence of cholesterol uptake; however, for days 5 and 7, the cells became strongly labeled, showing that LDL uptake was active.

Accumulation of cholesterol: Consistent with the upregulation of cholesterol and lipid synthetic pathways and lipid uptake in serum-deprived ARPE-19 cells, increased intracellular filipin labeling for unesterified cholesterol was seen in cells after 7 days in SFM, compared with cells grown for the same length of time in serum-containing medium (Figure 6A). In the serum-containing medium, most labeling was in the plasma membrane while in the SFM there was intense labeling within the cell. A quantitative assay for the total cell pellets confirmed the increased cholesterol labeling in the SFM (Figure 6B). In this assay, the majority of cholesterol in both conditions was identified as free, unesterified cholesterol, similar to results for other cell types [35,36].

Zinc-binding proteins and zinc supplementation: Another prominently regulated group of genes in ARPE-19 cells in SFM encodes ZBPs; Figure 2, Table 1 and Appendix 3). Several zinc-dependent enzymes and zinc-finger proteins were upregulated. Many have obscure function. For example, there is a large category of zinc-finger proteins many of which are predicted to have DNA or RNA binding activity but remain poorly characterized [37]. Notably, however, ZIP1/SLC39A1, the major zinc transporter [38], was upregulated while the cytoplasmic metal ion binding metallothioneins (MTs) decreased. MTs are sensitive markers of intracellular zinc levels and have roles in metal ion homeostasis and free radical scavenging [39]. Overall, these results were consistent with the decrease in free intracellular zinc and increased demand for zinc importation.

To test this, the expression levels of the genes for MTs, the zinc transporter, and other ZBP genes in ARPE-19 cells in SFM with and without zinc supplementation were compared at day 0, 1, 3, 5, 7, and 9 with qPCR (Figure 7, Appendix 6). With Zn^{2+} supplementation, the levels of MT gene expression increased significantly in SFM, consistent with a response to free zinc levels. As shown in Figure 7C, levels of protein for SLC39A1 in SFM increased by day 2–5, consistent with increased demand for zinc. Zinc supplementation led to a small decrease in the gene expression of the transporter. In contrast, serum deprivation/starvation-associated regulation of genes for two other ZBPs, FASN, and MARCH7, was not altered by zinc supplementation, suggesting they were not responding to zinc levels.

Primary fetal human RPE cells: Several key features of the serum deprivation model were also examined in primary fetal human RPE cells [25]. Similar to the ARPE-19 cells, the hfRPE cells survived for 7 days in DMEM SFM (Figure 8A). qPCR was used to examine expression profiles for several key DEGs from the ARPE-19 data. Similar trends were observed, with upregulation of lipid synthesis genes and downregulation of MT expression (Figure 8B), although over a shorter time scale of 1–2 days rather than 3–5 days as in the ARPE-19 cells. This result suggests that the responses in ARPE-19 cells may reflect a general stress program of the RPE cell lineage.

DISCUSSION

The RPE is a highly specialized, polarized monolayer located between the outer segments of the retinal photoreceptors and the vasculature of the choriocapillaris [1-3]. The RPE is essential for maintenance of the photoreceptors: phagocytosing shed disks, recycling components (most notably the vitamin A–derived visual pigment (retinal)), and mediating transport of nutrients and waste products between the outer retina and the blood supply. The RPE, with its underlying Bruch's membrane, also plays a key role in maintaining a physical barrier between the retina and the immune system and in preventing damage from inflammatory mechanisms. Healthy RPE has essentially no turnover, so cells must be able to maintain homeostasis while exposed to light and enduring the general stresses of aging. A major cause of vision loss in aging is AMD, a complex disease (or set of diseases) that involves RPE dysfunction [2,5,7,9] and is associated with damage to Bruch's membrane and loss of choroid capillaries [2,8]. Thus, it seems plausible that serum deprivation or starvation of the RPE and the outer retina may contribute to disease progression in AMD.

During the course of studies on the interaction of two AMD-relevant proteins, CFH and Fibulin 3, we noticed that RPE-derived ARPE-19 cells survived well under conditions of complete serum deprivation and secreted Fibulin 3 that is frequently observed in protein deposits associated with AMD [15]. As shown in this paper, ARPE-19 and primary human fetal RPE cells survive well without further feeding for several days in high-glucose SFM. Transcriptome analysis of confluent ARPE-19 cells in SFM showed that the major response to this deprivation was activation of pathways for lipid biosynthesis, particularly the sterol pathways. Supplementation with LDL blocked the upregulation of synthetic genes, but over the same time course, the major intracellular cholesterol transporter NPC1 [34] was upregulated and stayed at elevated levels even when the cells were supplemented with LDL. In addition to increased expression of cholesterol synthesis genes, ARPE-19 cells in SFM showed increased uptake of supplemental LDL. Filipin labeling showed a striking increase in the levels of intracellular unesterified cholesterol in confluent ARPE-19 cells in SFM, compared with cells grown for the same length of time in medium containing serum.

Although cholesterol homeostasis is an important mechanism in all cells, confluent cells deprived of cholesterol do not show upregulation of synthetic pathways or activation of the LDL receptor [40-42]. In contrast, confluent ARPE-19 cells respond to serum deprivation with upregulation of lipid synthesis, transport and uptake mechanisms, and accumulation of intracellular cholesterol. This response goes beyond homeostasis and suggests that it is a specific response to this form of stress. This is intriguing given the well established association of cholesterol and lipid deposits accumulating basal to RPE, at Bruch's membrane and in some drusen in AMD [7,15]. The functional significance of stress-related synthesis of cholesterol-rich material is not yet clear, but it could plausibly relate to processes such as increasing membrane fluidity and regulation of receptor-mediated processes [43] or modulating the toxic effects of misfolded protein deposits [44]. Modification of cholesterol-containing plasma membrane rafts has been implicated in several retinopathies [45,46].

In addition to the apparent increase in demand for cholesterol and lipids, serum deprivation of RPE-derived cells affects genes involved in binding and transport of zinc. In particular, metallothioneins were downregulated, consistent with a decrease in intracellular free zinc [39], while at the same time expression of the ZIP1/SLC39A1 zinc transporter [38] was upregulated. Zinc supplementation abolished the decrease in metallothioneins, consistent with their role in controlling levels of free zinc, while expression of zinc transporter declined only slightly. This result suggests that there

is an increased demand for zinc under serum deprivation, perhaps driven by increased levels of several stress-related zinc-binding proteins. The possible relevance of this for AMD arises from Age-Related Eye Disease Study (AREDS) population studies that have shown dietary zinc is protective against the disease [16].

ZBPs are plentiful with important regulatory functions. It is estimated that 40% of ZBPs are transcription factors with the remaining 60% comprised of enzymes or proteins involved in ion transport [47]. We performed a bioinformatics analysis of the differentially expressed zinc-binding proteins from the time series. Several of these ZBPs function in pathways that contribute to adaptive responses to stress (Table 1). Notably among the differentially expressed ZBPs that participate in apoptotic processes, those with increased expression (FBLIM1, FASN, RFWD2, RPS6KA5, NR2C2, and GLIS2) function to suppress apoptosis, while two apoptosis-implicated ZBPs that promote apoptosis (GLIS2 and JADE1) are downregulated. This result suggests that ARPE-19 cells may repress apoptosis during serum deprivation. Other ZBPs noted in Table 1 also have potentially important roles in RPE disease processes.

Another intriguing set of genes present in the list of differentially expressed genes are those with known associations with eye diseases (Table 2). Studies of gene networks have implicated disease genes as critical components of specialized functional pathways [48]. Although some of the genes in Table 2 have roles in cataract or other diseases not directly related to RPE, others could have roles in RPE cell homeostasis and stress response.

In AMD, the interface between the outer retina and the blood supply may be compromised in several ways. Significantly, the choroid capillaries themselves often regress [2,8] while Bruch's membrane thickens, and drusen and other deposits of proteins and lipids accumulate [2,5,7]. It is plausible that this leads to serum deprivation and starvation of RPE. As we have shown, ARPE-19 cells, which express RPE-specific markers and maintain many aspects of RPE morphology, show resilience to serum deprivation, and respond by accumulating cholesterol and increasing demand for zinc. Human fetal RPE cells behave in a similar way.

Although cell lines and primary cell cultures may differ from native tissues in their complete biologic context in some ways, they provide useful tools for exploring expression and response mechanisms that may be programmed in the cell lineage [49,50]. Thus, although eye-derived cell lines do not reproduce the fully differentiated state of complex tissues, such as the lens and the retina, these cell lines preserve many aspects of tissue-specific transcriptional activity and have been invaluable in characterizing gene expression mechanisms in complex eye tissues [51-53]. The serum deprivation and starvation response of cultured RPE cells may reflect a transcriptionally regulated program of the RPE lineage that could be activated during the progression of AMD. This would not be causative for AMD but might be adaptive for RPE under the stress of accumulating dysfunction in and around Bruch's membrane.

APPENDIX 1. *T* TESTS COMPARING GENE EXPRESSION ON DAY0 TO DAYS 1, 3, 5, AND 7 OF SERUM DEPRIVATION OF ARPE-19 AS DESCRIBED FOR EACH FEATURE OF THE NEIBANK CUSTOM HUMAN MICROARRAY. HCSID REFERS TO THE IN-HOUSE FEATURE ID, SYMBOL AND GENEID REFER TO THE ENTREZ IDS.

To access the data, click or select the words "Appendix 1."

APPENDIX 2. TEST COMPARING GENE EXPRESSION ON DAY0 TO DAY3 OF SERUM DEPRIVATION OF HEK-293 CELLS AS DESCRIBED FOR EACH FEATURE OF THE NEIBANK CUSTOM HUMAN MICROARRAY. HCSID REFERS TO THE IN-HOUSE FEATURE ID, SYMBOL AND GENEID REFER TO THE ENTREZ IDS.

To access the data, click or select the words "Appendix 2."

APPENDIX 3. *T* TEST RESULTS FROM THE SERUM STARVATION TIME SERIES OF ARPE-19 CELLS FILTERED FOR P VALUES LESS THAN 0.05 AND FOLD-CHANGE VALUES GREATER THAN +/− 1.2.

To access the data, click or select the words "Appendix 3."

APPENDIX 4. PROBE AND PRIMER COMBINATIONS USED FOR QPCR ASSAYS.

To access the data, click or select the words "Appendix 4."

APPENDIX 5. CONFIRMATION OF SELECTED MICROARRAY RESULTS BY QPCR.

Gene expression ratios of transcripts from ARPE-19 SFM cultures compared to Day0 serum supplemented cultures measured by qPCR. To access the data, click or select the words "Appendix 5."

APPENDIX 6. THE EFFECT OF ZINC SUPPLEMENTING SFM CULTURES OF ARPE-19.

Table of qPCR quantitation of metallothionein and zinc transporter gene expression in SFM ARPE19 cultures (SS) and Zn-supplemented SFM ARPE19 cultures (Zn). RQ=relative quantity. All values are relative to the Day0 serum supplemented value. Bar chart shows the gene expression values of the metallothionein genes and the zinc transporter SLC39A1 during SFM culture and Zn-supplemented SFM culture. The gray bars represent the Day0 calibrator value. Orange bars represent the sample ratio to day 0; bars extending above the gray bars indicate increased expression, bars ending below the gray bars indicate decreased expression. To access the data, click or select the words "Appendix 6."

ACKNOWLEDGMENTS

We thank Drs. Chun Gao and Maria Campos of NEI for expert help with microscopy and Dr. Cynthia Jaworski for helpful comments. We thank the laboratory of Dr. Sheldon Miller for human primary cells. This work was performed with support from the Intramural Program of the National Eye Institute, National Institutes of Health USA. **Author contributions**: GW, KP, and SM designed the studies and wrote the paper. Experiments were performed by SM, LY, KP, and JF. AB advised on experimental design and statistical analysis of gene expression.

REFERENCES

1. Bok D. The retinal pigment epithelium: a versatile partner in vision. J Cell Sci Suppl 1993; 17:189-95. [PMID: 8144697].
2. Bhutto I, Lutty G. Understanding age-related macular degeneration (AMD): relationships between the photoreceptor/retinal pigment epithelium/Bruch's membrane/choriocapillaris complex. Mol Aspects Med 2012; 33:295-317. [PMID: 22542780].
3. Strauss O. The retinal pigment epithelium in visual function. Physiol Rev 2005; 85:845-81. [PMID: 15987797].
4. Kur J, Newman EA, Chan-Ling T. Cellular and physiological mechanisms underlying blood flow regulation in the retina and choroid in health and disease. Prog Retin Eye Res 2012; 31:377-406. [PMID: 22580107].
5. Gehrs KM, Anderson DH, Johnson LV, Hageman GS. Age-related macular degeneration–emerging pathogenetic and therapeutic concepts. Ann Med 2006; 38:450-71. [PMID: 17101537].
6. Mullins RF, Russell SR, Anderson DH, Hageman GS. Drusen associated with aging and age-related macular degeneration contain proteins common to extracellular deposits associated with atherosclerosis, elastosis, amyloidosis, and dense deposit disease. FASEB J 2000; 14:835-46. [PMID: 10783137].
7. Curcio CA, Johnson M, Rudolf M, Huang JD. The oil spill in ageing Bruch membrane. Br J Ophthalmol 2011; 95:1638-45. [PMID: 21890786].
8. Mullins RF, Khanna A, Schoo DP, Tucker BA, Sohn EH, Drack AV, Stone EM. Is age-related macular degeneration a microvascular disease? Adv Exp Med Biol 2014; 801:283-9. [PMID: 24664709].
9. Zarbin MA. Current concepts in the pathogenesis of age-related macular degeneration. Arch Ophthalmol 2004; 122:598-614. [PMID: 15078679].
10. Newman AM, Gallo NB, Hancox LS, Miller NJ, Radeke CM, Maloney MA, Cooper JB, Hageman GS, Anderson DH, Johnson LV, Radeke MJ. Systems-level analysis of age-related macular degeneration reveals global biomarkers and phenotype-specific functional networks. Genome Med 2012; 4:16-[PMID: 22364233].
11. Chen W, Stambolian D, Edwards AO, Branham KE, Othman M, Jakobsdottir J, Tosakulwong N, Pericak-Vance MA, Campochiaro PA, Klein ML, Tan PL, Conley YP, Kanda A, Kopplin L, Li Y, Augustaitis KJ, Karoukis AJ, Scott WK, Agarwal A, Kovach JL, Schwartz SG, Postel EA, Brooks M, Baratz KH, Brown WL, Brucker AJ, Orlin A, Brown G, Ho A, Regillo C, Donoso L, Tian L, Kaderli B, Hadley D, Hagstrom SA, Peachey NS, Klein R, Klein BE, Gotoh N, Yamashiro K, Ferris Iii F, Fagerness JA, Reynolds R, Farrer LA, Kim IK, Miller JW, Corton M, Carracedo A, Sanchez-Salorio M, Pugh EW, Doheny KF, Brion M, Deangelis MM, Weeks DE, Zack DJ, Chew EY, Heckenlively JR, Yoshimura N, Iyengar SK, Francis PJ, Katsanis N, Seddon JM, Haines JL, Gorin MB, Abecasis GR, Swaroop A. Genetic variants near TIMP3 and high-density lipoprotein-associated loci influence susceptibility to age-related macular degeneration. Proc Natl Acad Sci USA 2010; 107:7401-6. [PMID: 20385819].
12. Kaneko H, Dridi S, Tarallo V, Gelfand BD, Fowler BJ, Cho WG, Kleinman ME, Ponicsan SL, Hauswirth WW, Chiodo VA, Kariko K, Yoo JW, Lee DK, Hadziahmetovic M, Song Y, Misra S, Chaudhuri G, Buaas FW, Braun RE, Hinton DR, Zhang Q, Grossniklaus HE, Provis JM, Madigan MC, Milam AH, Justice NL, Albuquerque RJ, Blandford AD, Bogdanovich S, Hirano Y, Witta J, Fuchs E, Littman DR, Ambati BK, Rudin CM, Chong MM, Provost P, Kugel JF, Goodrich JA, Dunaief JL, Baffi JZ, Ambati J. DICER1 deficit induces Alu RNA toxicity in age-related macular degeneration. Nature 2011; 471:325-30. [PMID: 21297615].
13. Klein R, Peto T, Bird A, Vannewkirk MR. The epidemiology of age-related macular degeneration. Am J Ophthalmol 2004; 137:486-95. [PMID: 15013873].
14. Zanzottera EC, Messinger JD, Ach T, Smith RT, Freund KB, Curcio CA. The Project MACULA Retinal Pigment Epithelium Grading System for Histology and Optical Coherence Tomography in Age-Related Macular Degeneration. Invest Ophthalmol Vis Sci 2015; 56:3253-68. [PMID: 25813989].
15. Wyatt MK, Tsai JY, Mishra S, Campos M, Jaworski C, Fariss RN, Bernstein SL, Wistow G. Interaction of complement

factor h and fibulin3 in age-related macular degeneration. PLoS One 2013; 8:e68088-[PMID: 23840815].

16. Chew EY. Nutrition effects on ocular diseases in the aging eye. Invest Ophthalmol Vis Sci 2013; 54:ORSF42-7. [PMID: 24335067].

17. Dunn KC, Aotaki-Keen AE, Putkey FR, Hjelmeland LM. ARPE-19, a human retinal pigment epithelial cell line with differentiated properties. Exp Eye Res 1996; 62:155-69. [PMID: 8698076].

18. Marmorstein LY, Munier FL, Arsenijevic Y, Schorderet DF, McLaughlin PJ, Chung D, Traboulsi E, Marmorstein AD. Aberrant accumulation of EFEMP1 underlies drusen formation in Malattia Leventinese and age-related macular degeneration. Proc Natl Acad Sci USA 2002; 99:13067-72. [PMID: 12242346].

19. Sekiyama E, Saint-Geniez M, Yoneda K, Hisatomi T, Nakao S, Walshe TE, Maruyama K, Hafezi-Moghadam A, Miller JW, Kinoshita S, D'Amore PA. Heat treatment of retinal pigment epithelium induces production of elastic lamina components and antiangiogenic activity. FASEB J 2012; 26:567-75. [PMID: 22067481].

20. Samuel W, Kutty RK, Duncan T, Vijayasarathy C, Kuo BC, Chapa KM, Redmond TM. Fenretinide induces ubiquitin-dependent proteasomal degradation of stearoyl-CoA desaturase in human retinal pigment epithelial cells. J Cell Physiol 2014; 229:1028-38. [PMID: 24357007].

21. Karlsson M, Kurz T. Attenuation of iron-binding proteins in ARPE-19 cells reduces their resistance to oxidative stress. Acta Ophthalmol 2016; [PMID: 27287874].

22. Olchawa MM, Pilat AK, Szewczyk GM, Sarna TJ. Inhibition of phagocytic activity of ARPE-19 cells by free radical mediated oxidative stress. Free Radic Res 2016; 50:1-11. [PMID: 27225587].

23. Koskela A, Reinisalo M, Petrovski G, Sinha D, Olmiere C, Karjalainen R, Kaarniranta K. Nutraceutical with Resveratrol and Omega-3 Fatty Acids Induces Autophagy in ARPE-19 Cells. Nutrients 2016; 8:[PMID: 27187449].

24. Gangalum RK, Bhat AM, Kohan SA, Bhat SP. Inhibition of the Expression of the Small Heat Shock Protein αB-Crystallin Inhibits Exosome Secretion in Human Retinal Pigment Epithelial Cells in Culture. J Biol Chem 2016; 291:12930-42. [PMID: 27129211].

25. Maminishkis A, Chen S, Jalickee S, Banzon T, Shi G, Wang FE, Ehalt T, Hammer JA, Miller SS. Confluent monolayers of cultured human fetal retinal pigment epithelium exhibit morphology and physiology of native tissue. Invest Ophthalmol Vis Sci 2006; 47:3612-24. [PMID: 16877436].

26. Livak KJ, Schmittgen TD. Analysis of relative gene expression data using real-time quantitative PCR and the 2ˆ(-Delta Delta Ct) Method. Methods 2001; 25:402-8. [PMID: 11846609].

27. Thompson RB, Reffatto V, Bundy JG, Kortvely E, Flinn JM, Lanzirotti A, Jones EA, McPhail DS, Fearn S, Boldt K, Ueffing M, Ratu SG, Pauleikhoff L, Bird AC, Lengyel I. Identification of hydroxyapatite spherules provides new insight into subretinal pigment epithelial deposit formation in the aging eye. Proc Natl Acad Sci USA 2015; 112:1565-70. [PMID: 25605911].

28. Li Y, Song D, Song Y, Zhao L, Wolkow N, Tobias JW, Song W, Dunaief JL. Iron-induced Local Complement Component 3 (C3) Up-regulation via Non-canonical Transforming Growth Factor (TGF)-beta Signaling in the Retinal Pigment Epithelium. J Biol Chem 2015; 290:11918-34. [PMID: 25802332].

29. Gangalum RK, Atanasov IC, Zhou ZH, Bhat SP. AlphaB-crystallin is found in detergent-resistant membrane microdomains and is secreted via exosomes from human retinal pigment epithelial cells. J Biol Chem 2011; 286:3261-9. [PMID: 21097504].

30. Wistow G. The NEIBank project for ocular genomics: Data-mining gene expression in human and rodent eye tissues. Prog Retin Eye Res 2005; 25:43-77. [PMID: 16005676].

31. Wistow G, Peterson K, Gao J, Buchoff P, Jaworski C, Bowes-Rickman C, Ebright JN, Hauser MA, Hoover D. NEIBank: genomics and bioinformatics resources for vision research. Mol Vis 2008; 14:1327-37. [PMID: 18648525].

32. Bommer GT, MacDougald OA. Regulation of lipid homeostasis by the bifunctional SREBF2-miR33a locus. Cell Metab 2011; 13:241-7. [PMID: 21356514].

33. Castoreno AB, Wang Y, Stockinger W, Jarzylo LA, Du H, Pagnon JC, Shieh EC, Nohturfft A. Transcriptional regulation of phagocytosis-induced membrane biogenesis by sterol regulatory element binding proteins. Proc Natl Acad Sci USA 2005; 102:13129-34. [PMID: 16141315].

34. King G, Sharom FJ. Proteins that bind and move lipids: MsbA and NPC1. Crit Rev Biochem Mol Biol 2012; 47:75-95. [PMID: 22117698].

35. Robinet P, Wang Z, Hazen SL, Smith JD. A simple and sensitive enzymatic method for cholesterol quantification in macrophages and foam cells. J Lipid Res 2010; 51:3364-9. [PMID: 20688754].

36. Csoka B, Koscso B, Toro G, Kokai E, Virag L, Nemeth ZH, Pacher P, Bai P, Hasko G. A2B adenosine receptors prevent insulin resistance by inhibiting adipose tissue inflammation via maintaining alternative macrophage activation. Diabetes 2014; 63:850-66. [PMID: 24194503].

37. Krishna SS, Majumdar I, Grishin NV. Structural classification of zinc fingers: survey and summary. Nucleic Acids Res 2003; 31:532-50. [PMID: 12527760].

38. Jeong J, Eide DJ. The SLC39 family of zinc transporters. Mol Aspects Med 2013; 34:612-9. [PMID: 23506894].

39. Maret W. Metallothionein redox biology in the cytoprotective and cytotoxic functions of zinc. Exp Gerontol 2008; 43:363-9. [PMID: 18171607].

40. Ho YK, Faust JR, Bilheimer DW, Brown MS, Goldstein JL. Regulation of cholesterol synthesis by low density lipoprotein in isolated human lymphocytes. Comparison of cells from normal subjects and patients with homozygous familial hypercholesterolemia and abetalipoproteinemia. J Exp Med 1977; 145:1531-49. [PMID: 194011].

41. Kruth HS, Avigan J, Gamble W, Vaughan M. Effect of cell density on binding and uptake of low density lipoprotein by human fibroblasts. J Cell Biol 1979; 83:588-94. [PMID: 230192].

42. Gal D, MacDonald PC, Porter JC, Smith JW, Simpson ER. Effect of cell density and confluency on cholesterol metabolism in cancer cells in monolayer culture. Cancer Res 1981; 41:473-7. [PMID: 7448794].

43. Yao Y, Hong S, Zhou H, Yuan T, Zeng R, Liao K. The differential protein and lipid compositions of noncaveolar lipid microdomains and caveolae. Cell Res 2009; 19:497-506. [PMID: 19255590].

44. Evangelisti E, Cecchi C, Cascella R, Sgromo C, Becatti M, Dobson CM, Chiti F, Stefani M. Membrane lipid composition and its physicochemical properties define cell vulnerability to aberrant protein oligomers. J Cell Sci 2012; 125:2416-27. [PMID: 22344258].

45. Filomenko R, Fourgeux C, Bretillon L, Gambert-Nicot S. Oxysterols: Influence on plasma membrane rafts microdomains and development of ocular diseases. Steroids 2015; 99:259-65.. [PMID: 25683893].

46. Wang L, Li CM, Rudolf M, Belyaeva OV, Chung BH, Messinger JD, Kedishvili NY, Curcio CA. Lipoprotein particles of intraocular origin in human Bruch membrane: an unusual lipid profile. Invest Ophthalmol Vis Sci 2009; 50:870-7. [PMID: 18806290].

47. Ebert JC, Altman RB. Robust recognition of zinc binding sites in proteins. Protein Sci 2008; 17:54-65. [PMID: 18042678].

48. Goh KI, Cusick ME, Valle D, Childs B, Vidal M, Barabasi AL. The human disease network. Proc Natl Acad Sci USA 2007; 104:8685-90. [PMID: 17502601].

49. Consortium EP. An integrated encyclopedia of DNA elements in the human genome. Nature 2012; 489:57-74. [PMID: 22955616].

50. Consortium EP. A user's guide to the encyclopedia of DNA elements (ENCODE). PLoS Biol 2011; 9:e1001046-[PMID: 21526222].

51. Cvekl A, Yang Y, Chauhan BK, Cveklova K. Regulation of gene expression by Pax6 in ocular cells: a case of tissue-preferred expression of crystallins in lens. Int J Dev Biol 2004; 48:829-44. [PMID: 15558475].

52. Merbs SL, Khan MA, Hackler L Jr, Oliver VF, Wan J, Qian J, Zack DJ. Cell-specific DNA methylation patterns of retina-specific genes. PLoS One 2012; 7:e32602-[PMID: 22403679].

53. Khanna H, Akimoto M, Siffroi-Fernandez S, Friedman JS, Hicks D, Swaroop A. Retinoic acid regulates the expression of photoreceptor transcription factor NRL. J Biol Chem 2006; 281:27327-34. [PMID: 16854989].

54. Zhao J, Zhang Y, Ithychanda SS, Tu Y, Chen K, Qin J, Wu C. Migfilin interacts with Src and contributes to cell-matrix adhesion-mediated survival signaling. J Biol Chem 2009; 284:34308-20. [PMID: 19833732].

55. Jung SY, Jeon HK, Choi JS, Kim YJ. Reduced expression of FASN through SREBP-1 down-regulation is responsible for hypoxic cell death in HepG2 cells. J Cell Biochem 2012; 113:3730-9. [PMID: 22786746].

56. Love IM, Grossman SR. It Takes 15 to Tango: Making Sense of the Many Ubiquitin Ligases of p53. Genes Cancer 2012; 3:249-63. [PMID: 23150758].

57. Marine JC. Spotlight on the role of COP1 in tumorigenesis. Nat Rev Cancer 2012; 12:455-64. [PMID: 22673153].

58. Kobayashi S, Yoneda-Kato N, Itahara N, Yoshida A, Kato JY. The COP1 E3-ligase interacts with FIP200, a key regulator of mammalian autophagy. BMC Biochem 2013; 14:1-[PMID: 23289756].

59. Sundar IK, Chung S, Hwang JW, Lapek JD Jr, Bulger M, Friedman AE, Yao H, Davie JR, Rahman I. Mitogen- and stress-activated kinase 1 (MSK1) regulates cigarette smoke-induced histone modifications on NF-kappaB-dependent genes. PLoS One 2012; 7:e31378-[PMID: 22312446].

60. Kunchithapautham K, Atkinson C, Rohrer B. Smoke-exposure causes endoplasmic reticulum stress and lipid accumulation in retinal pigment epithelium through oxidative stress and complement activation. J Biol Chem 2014; 289:14534-46. [PMID: 24711457].

61. Cano M, Thimmalappula R, Fujihara M, Nagai N, Sporn M, Wang AL, Neufeld AH, Biswal S, Handa JT. Cigarette smoking, oxidative stress, the anti-oxidant response through Nrf2 signaling, and Age-related Macular Degeneration. Vision Res 2010; 50:652-64. [PMID: 19703486].

62. SanGiovanni JP, Lee PH. AMD-associated genes encoding stress-activated MAPK pathway constituents are identified by interval-based enrichment analysis. PLoS One 2013; 8:e71239-[PMID: 23940728].

63. Attanasio M, Uhlenhaut NH, Sousa VH, O'Toole JF, Otto E, Anlag K, Klugmann C, Treier AC, Helou J, Sayer JA, Seelow D, Nurnberg G, Becker C, Chudley AE, Nurnberg P, Hildebrandt F, Treier M. Loss of GLIS2 causes nephronophthisis in humans and mice by increased apoptosis and fibrosis. Nat Genet 2007; 39:1018-24. [PMID: 17618285].

64. Kim YS, Kang HS, Herbert R, Beak JY, Collins JB, Grissom SF, Jetten AM. Kruppel-like zinc finger protein Glis2 is essential for the maintenance of normal renal functions. Mol Cell Biol 2008; 28:2358-67. [PMID: 18227149].

65. Zhou MI, Foy RL, Chitalia VC, Zhao J, Panchenko MV, Wang H, Cohen HT. Jade-1, a candidate renal tumor suppressor that promotes apoptosis. Proc Natl Acad Sci USA 2005; 102:11035-40. [PMID: 16046545].

66. Thomas JL, Vihtelic TS, denDekker AD, Willer G, Luo X, Murphy TR, Gregg RG, Hyde DR, Thummel R. The loss of vacuolar protein sorting 11 (vps11) causes retinal pathogenesis in a vertebrate model of syndromic albinism. Invest Ophthalmol Vis Sci 2011; 52:3119-28. [PMID: 21330665].

67. Li Y, Yang D, Bai Y, Mo X, Huang W, Yuan W, Yin Z, Deng Y, Murashko O, Wang Y, Fan X, Zhu C, Ocorr K, Bodmer R, Wu X. ZNF418, a novel human KRAB/C2H2 zinc finger

protein, suppresses MAPK signaling pathway. Mol Cell Biochem 2008; 310:141-51. [PMID: 18084723].

68. Luhmann UF, Robbie SJ, Bainbridge JW, Ali RR. The relevance of chemokine signalling in modulating inherited and age-related retinal degenerations. Adv Exp Med Biol 2014; 801:427-33. [PMID: 24664727].

Articles are provided courtesy of Emory University and the Zhongshan Ophthalmic Center, Sun Yat-sen University, P.R. China. The print version of this article was created on 10 December 2016. This reflects all typographical corrections and errata to the article through that date. Details of any changes may be found in the online version of the article.